Available online at www.sciencedirect.com
SCIENCE DIRECT®
ELSEVIER
Acta Materialia 52 (2004) 2047–2056
Acta MATERIALIA
www.actamat-journals.com

Solid state interfacial reaction of Sn–37Pb and Sn–3.5Ag solders with Ni–P under bump metallization

Min He [a], Zhong Chen [a,*], Guojun Qi [b]

[a] *School of Materials Engineering, Nanyang Technological University, Nanyang Avenue, Singapore 639798, Singapore*
[b] *Singapore Institute of Manufacturing Technology, 71 Nanyang Drive, Singapore 638075, Singapore*

Received 15 October 2003; received in revised form 24 December 2003; accepted 24 December 2003

Abstract

Thermal aging is one of the accelerated tests for IC package reliability during manufacturing processes and under actual usage conditions. During the process of thermal aging, intermetallic compounds (IMC) grow continuously due to element diffusion, resulting in their morphology change and thickness increase. In this work, the solid state reaction between electroless Ni–P and two types of Sn-based solders (Sn–3.5Ag and Sn–37Pb) has been investigated. Three distinctive layers, Ni_3Sn_4, NiSnP and Ni_3P, were found between the Sn-containing solders and Ni–P under bump metallization. The growth rates of Ni_3Sn_4 IMC at different temperatures were obtained from the aged samples and the activation energy of Ni_3Sn_4 growth was estimated. The kinetic data obtained show that the Ni_3Sn_4 in the Sn–3.5Ag/Ni–P joints grows much faster than with the Sn–37Pb solder under the same condition. Kirkendall voids are found inside the Ni_3P layer after thermal aging. The void formation mechanism is due to net Ni out-flux into the solder area.
© 2004 Acta Materialia Inc. Published by Elsevier Ltd. All rights reserved.

Keywords: Lead-free solder; Electroless Ni–P; Intermetallic compound; Kirkendall voids; Diffusion

1. Introduction

Selection of appropriate under bump metallization (UBM) plays an important role in developing a reliable flip chip packaging technology. This is especially so with the adoption of lead-free solders in the solder joints. Copper based UBM works well with Sn-based high lead solders. However, reliability concerns arise when it is used together with high Sn content solders due to rapid consumption of Cu and spallation of Cu–Sn intermetallic compounds (IMCs) [1–4]. As alternatives, Ni-based under bump metallizations, such as electroless nickel (EN), have been reported to have slower chemical reactions with the high-Sn solders as compared to Cu-based UBM [2]. EN, which is an alloy of Ni and P, has attracted a great deal of attention because of its good solderability and low process cost [5,6]. Many studies have been published on the interaction between Ni–P and Sn-based solders [7–17]. Topics of these studies include formation and growth of IMCs at the interface between molten solder and Ni–P UBM [7–9], solder reaction-assisted crystallization of electroless Ni–P alloy [10–12], and the influences of the IMCs on the mechanical properties of the solder joints [13–15].

In soldering reflow process, the reaction result of Sn-containing solders and electroless Ni–P UBM is the formation of Ni_3Sn_4 IMC layer between solder and UBM [1,2,5]. A P-rich layer also formed between Ni_3Sn_4 and Ni–P UBM [9]. Jang et al. [10] studied the reaction between Ni–P and eutectic Sn–Pb solder in reflow process. They reported that the P-rich layer consisted of Ni_3P. Zeng and Tu [1] reflowed SnAgCu solder with Ni–P UBM for five times and found a Ni–Sn–P ternary phase between Ni_3Sn_4 and Ni_3P layers. In addition, they found Kirkendall voids in the SnAgCu/Ni–P UBM system [1]. Jeon et al. [17] used TEM to study the reaction of Ni–P UBM with both Sn–Pb and Sn–Ag solders in liquid state reaction. However, they observed Kirkendall voids inside Ni_3Sn_4 layer at the locations

* Corresponding author. Tel.: +65-6790-4256; fax: +65-6790-9081.
E-mail address: aszchen@ntu.edu.sg (Z. Chen).

1359-6454/$30.00 © 2004 Acta Materialia Inc. Published by Elsevier Ltd. All rights reserved.
doi:10.1016/j.actamat.2003.12.042

close to Ni_3P, but not inside the Ni_3P layer. In summary, various findings, some of which may not be in agreement with each other, have been reported on the interfacial reaction between different types of solder with Ni–P UBM. Different observation leads to different explanation in the mechanisms of interfacial reaction.

So far, most of reports on solder/Ni–P reaction are based on liquid state reaction in reflow process. Less understood is the solid state reaction of the joints at relatively high temperatures. For example, solid state aging at 150 °C for 1000 h is a required reliability test. In certain applications, such as under the hood of an automobile, IC packages may work continuously in a high temperature environment. Although the general prediction based on common knowledge will be true that the IMCs will keep growing at a slower speed in solid state, it warrants more detailed studies on the behavior of the Sn-based solder joints with Ni–P UBM to address the concerns on the influence of the solid state reaction on the reliability of packages. Solid state reaction at high temperature with extended annealing time has an additional advantage of revealing details of interfacial reactions so that a better understanding of the reaction mechanisms can be reached.

In this paper, we report our experimental results of solid state reaction between Ni–P UMB and two types of Sn-based solders, eutectic Sn–37Pb and lead-free Sn–3.5Ag alloys. The growth kinetics of Ni–Sn intermetallics and also the effect of aging temperature and time on the morphology of IMCs are examined. By comparing these two alloys with different Sn concentration, the role of Sn in the interfacial reaction will be better understood. An observation of Kirkendall voids in one of the interfacial layers is of special significance for the solid state reaction. The formation and growth mechanisms of the voids have been proposed. We will also attempt to elucidate the mechanisms of interfacial reaction between Sn-containing solders and Ni–P UBM.

2. Experimental procedures

2.1. UBM preparation

The substrates used in this study were prepared from blank Si wafers. 1000-Å-thick chromium layer was sputtered first, followed by sputter deposition of about 1 μm nickel and 0.1 μm gold. The chromium provides good adhesion of the UBM to the wafer. The pure nickel was used as the seed layer for the subsequent electroless nickel plating and the gold is for protection of nickel from oxidation. Ni–P (containing 12.5 at.% P) UBM of about 5 μm was obtained by electroless plating with a commercial solution on the above mentioned sputtered nickel substrate. Before the plating, the sputtered gold layer was etched away. A final finish of immersion gold on the plated Ni–P was applied as a surface protection.

2.2. Reflow and thermal aging process

Both eutectic Sn–37Pb solder and Sn–3.5Ag solder are in the form of wire with no-clean reflow flux in the core. In a reflow process of the experiment, 30 mg of the solder wire was placed in contact with the Ni–P coated substrate and then sent into a reflow oven. Three thermocouples, two attached to the sample and one fixed on the oven ceiling, were used to monitor the temperature change during the reflow process. The Sn–3.5Ag sample was heated to a peak temperature of 251 °C and kept for 180 s, while eutectic Sn–37Pb was heated to and kept at 213 °C for 120 s. The maximum temperature is chosen to be 30 °C above their respective melting points.

Selected Sn–3.5Ag solder samples reflowed for 180 s were thermally aged at 130, 150, 170 and 190 °C for 100, 225, 400 and 625 h in air atmosphere. Similarly, selected eutectic Sn–37Pb solder samples reflowed for 120 s were thermally aged at 130, 150 and 170 °C for the same aging period. Some Sn–3.5Ag samples were aged at 216 °C for the purpose of observing Kirkendall voids at such an extreme condition.

2.3. Observation of reacted products at interface

Reflowed and thermal aged samples were prepared for observations of cross-sectional structure and top view (looking from the solder bulk to the solder/UBM interface) of the IMC morphology under SEM. The common metallography practice was followed to reveal the cross-sectional microstructure. The average thickness of the IMC was obtained for each sample by measuring the cross-section area of the layer over a certain length on the SEM image with the help of an image analyzer. In order to obtain the top view of intermetallic compounds, majority of the solder on the specimens were first ground away, then the specimens were etched with 2% HCl for 30 min to selectively dissolve the remaining solder.

The microstructure of interfacial reaction region between solder and Ni–P UBM was investigated by cross-sectional transmission electron microscopy (XTEM) combined with energy dispersive X-ray spectroscopy (EDX). TEM samples were prepared by diamond saw cutting to the thickness around 200 μm and then grinding using double-side mechanical dimpling. A thin area of around 20 μm could be achieved in the center by this approach. A cold-stage Ar^+ ion milling at liquid nitrogen temperature was used to prevent the sample from high temperature damage. TEM observations were performed using a JEOL JEM 2010 microscope operating at 200 kV. A microprobe beam of $\sim$10 nm in

diameter was used for the composition analysis using EDX.

3. Results

3.1. Morphology of intermetallic compounds in as-reflowed samples

Typical cross-sectional and top views of the intermetallic compounds formed after reflow are shown in Fig. 1 (Sn–3.5Ag) and Fig. 2 (Sn–37Pb). The same basic structure is observed at the interfaces between the UBM and two solders: in contact with the Ni–P UBM is a layer of P-rich phase with the P content close to the stoichiometry of Ni_3P. TEM analysis confirmed that this layer is dominated by nanocrystalline phase of Ni_3P. This layer will be addressed as Ni_3P layer in the following text. In between the Ni_3P and bulk solder is a relatively thick IMC layer which is confirmed to be Ni_3Sn_4, irrespective of their shape and sizes. This is in agreement with what was reported by Jang et al. [10,16] and Jeon et al. [17]. Some Ag_3Sn agglomerates are seen dispersed randomly in the Sn–3.5Ag solder matrix.

From the top structural micrographs in Fig. 1(b) and Fig. 2(b), chunk-type and needle-type Ni_3Sn_4 IMC grains can be observed in both Sn–3.5Ag and Sn–37Pb solder systems. The morphology differences are, however, quite obvious: with the Sn–37Pb solder, the amount and size of chunk-type IMC grains are less than those with Sn–3.5Ag solder. From the cross-sectional view of Sn–3.5Ag samples, the Ni_3Sn_4 IMC layer appears to have chunky protrusions into the bulk solder while the intermetallics of SnPb system has more needle-type spikes.

3.2. Morphology and growth kinetics of Ni_3Sn_4 intermetallic compounds in solid state reaction

The interfacial reaction of the solders with the Ni–P UBMs continues during thermal aging process. This is

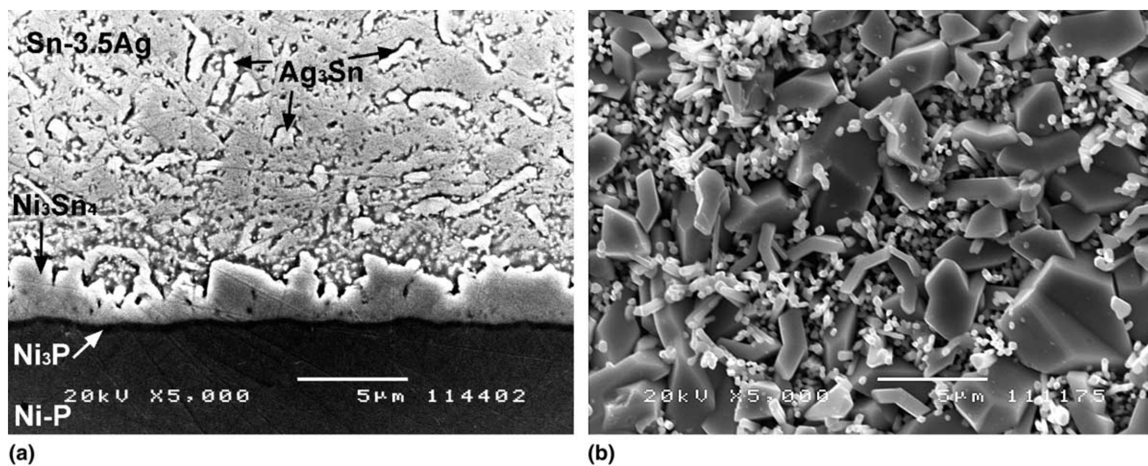

Fig. 1. Morphology of Ni_3Sn_4 IMC in Sn–3.5Ag solder and Ni–P UBM system after reflow. (a) Cross-section. (b) Top view.

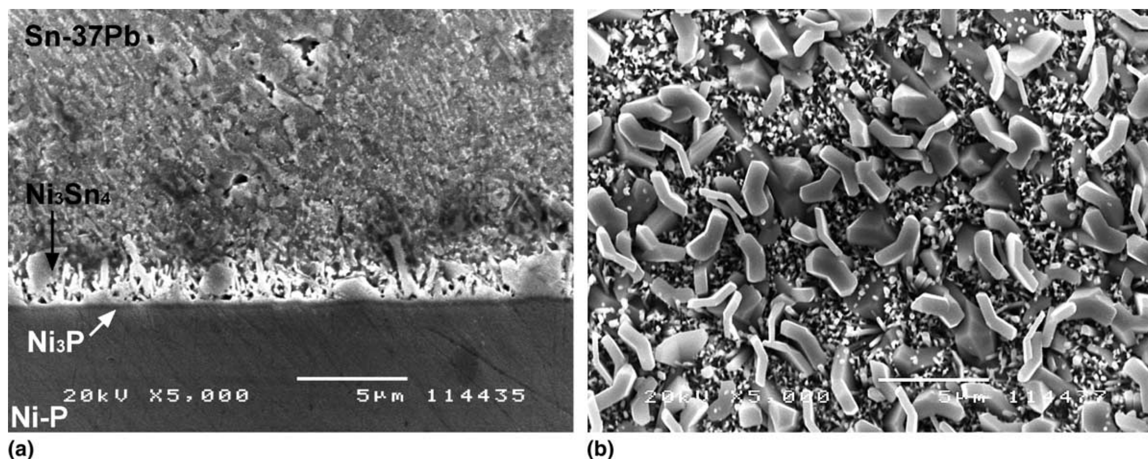

Fig. 2. Morphology of Ni_3Sn_4 IMC in Sn–37Pb solder and Ni–P UBM system after reflow. (a) Cross-section. (b) Top view.

evidenced by the morphology change and thickness increase of the IMCs as compared to the as-reflowed state. The cross-sectional views of the Ni_3Sn_4 are shown in Fig. 3. Ni_3Sn_4 IMC becomes flatter and thicker after aging than in the as-reflowed samples. For Sn–3.5Ag solder samples, the interface of the IMC layers with the amorphous Ni–P became more crooked, implying more consumption of the electroless Ni–P in certain locations when forming the additional IMCs during the thermal aging.

The top view micrographs of Ni_3Sn_4 IMC after 400-h aging at 130 °C are shown in Fig. 4. Only chunk-type IMC can be found in these samples. The surface of the IMC becomes flatter although the facets are still visible. The IMC grain size of the Sn–3.5Ag solder is larger than that of the eutectic SnPb solder. From the micrographs it appears that the neighboring IMC grains are merging with each other, which can be appreciated from those disappearing grain boundaries arrowed in Fig. 4. This mechanism has been described elsewhere [18].

The thickness of the Ni_3Sn_4 layer is found to increase linearly with square root of aging time and grows faster at higher temperatures. The results are shown in Fig. 5 and the linear coefficients are listed in Table 1. The IMC growth rates in Sn–3.5Ag solder system are much faster than those in Sn–37Pb.

3.3. Formation of Kirkendall voids

Kirkendall voids have been observed inside the Ni_3P layer under SEM. Typical views of such voids are shown in Figs. 6 and 7. The SEM-observable voids and their sizes depend on the thermal aging temperature and duration. No voids were observed under SEM in the samples aged at 130 °C for as long as 625 h in both Sn–3.5Ag and Sn–37Pb samples. The voids can only be

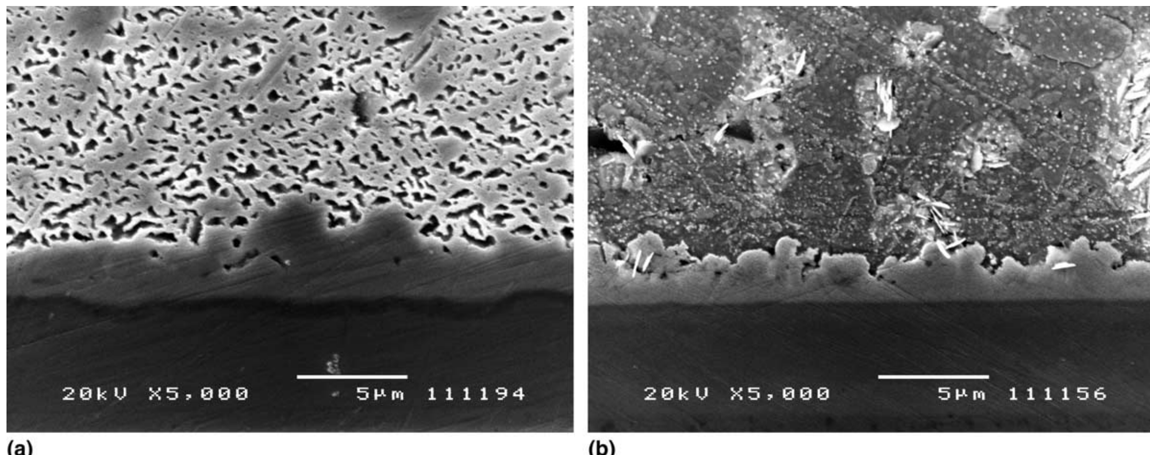

Fig. 3. Ni_3Sn_4 IMCs formed between Sn-rich solders and Ni–P UBM after 100 h aging at 130 °C. (a) Sn–3.5Ag with Ni–P UBM. (b) Sn–37Pb with Ni–P UBM.

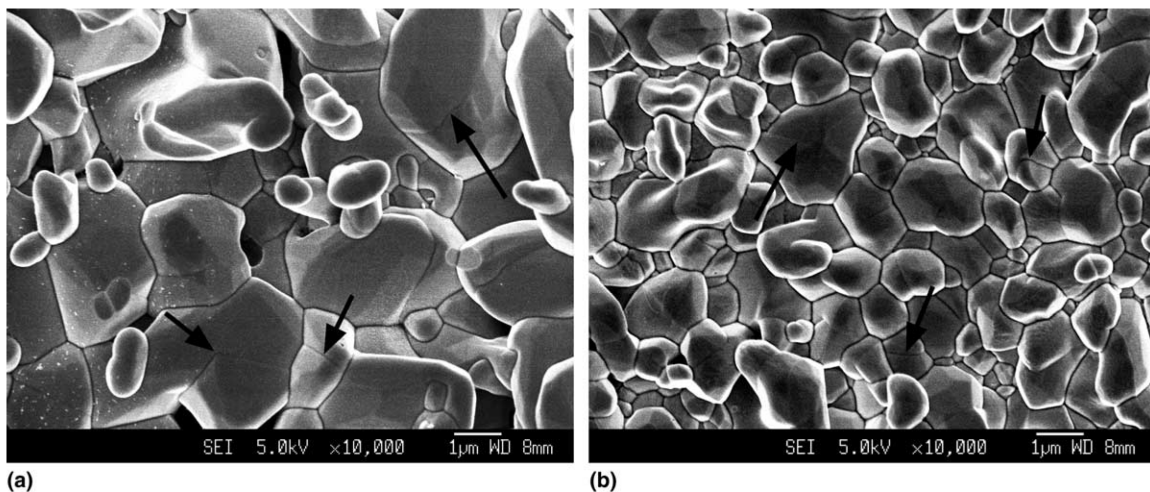

Fig. 4. Ni_3Sn_4 IMCs formed between Sn-rich solders and Ni–P UBM after 400 h aging at 130 °C. (a) Sn–3.5Ag with Ni–P UBM. (b) Sn–37Pb with Ni–P UBM.

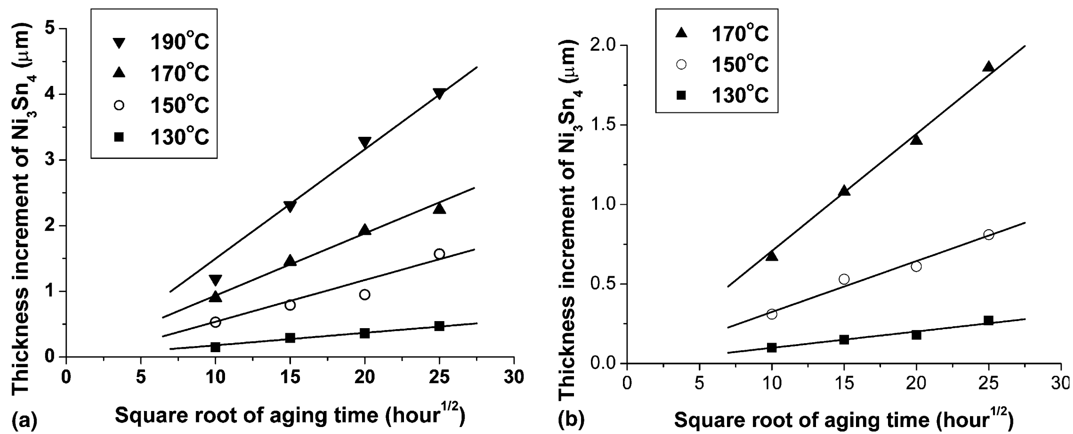

Fig. 5. Ni_3Sn_4 growth for Sn–3.5Ag and Sn–37Pb solders with Ni–P UBM in solid state reaction. (a) Sn–3.5Ag with Ni–P UBM. (b) Sn–37Pb with Ni–P UBM.

Table 1
IMC growth constants (cm^2/s) for Sn–3.5Ag, Sn–37Pb solders and Ni–P UBM

Solder	130 °C	150 °C	170 °C	190 °C
Sn–3.5Ag	9.99×10^{-16}	1.12×10^{-14}	2.49×10^{-14}	7.70×10^{-14}
Sn–37Pb	3.61×10^{-16}	4.40×10^{-15}	1.44×10^{-14}	–

found after long period aging at 150 °C for both solder systems. For temperatures at 170 °C and above, voids were observed after a relatively short aging time (Figs. 6 and 7). By comparing Fig. 6(a) with Fig. 6(b) as well as Fig. 7(a) with Fig. 7(b), it is clear that the size and amount of voids increase with aging time.

For lower temperatures and shorter period of aging, Kirkendall voids can only be observed with TEM. Fig. 8(a) is a bright field TEM image from the Ni_3P region of a Sn–3.5Ag sample that has been aged at 150 °C for 100 h. It can be seen that the Ni_3P layer shows a well-developed fine columnar structure, which will be discussed later. Voids of different sizes, labeled as region A, B and C in Fig. 8(a), can be found inside this layer. All these small voids are difficult to observe with SEM. TEM observation seems to suggest that these voids tend to form an elliptical shape with its main axis aligned along the columnar direction.

3.4. NiSnP phase in between Ni_3Sn_4 and Ni_3P

Careful examination on samples after long time thermal aging at high temperatures revealed that another phase containing Sn, Ni and P exists in between the Ni_3Sn_4 and Ni_3P. A detailed identification of the microstructure of this layer is still on going. Therefore for the time being, we name it NiSnP phase (or layer) and preliminary results are presented here. A typical SEM view for the NiSnP layer is shown in Fig. 9(a) and the schematic diagram is shown in Fig. 9(b). A much thinner (than the Ni_3P layer), yet clearly visible grey layer exists in between the dark Ni_3P and the bright

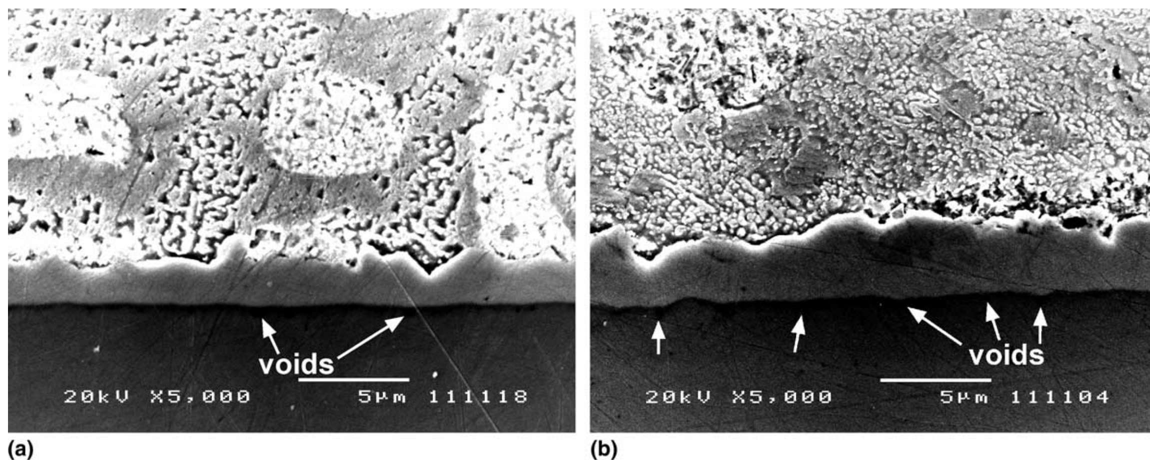

Fig. 6. Kirkendall voids began to form in samples of Sn–37Pb solder with Ni–P UBM aged at 170 °C. Voids grow with aging time at fixed temperature. (a) 100 h. (b) 625 h.

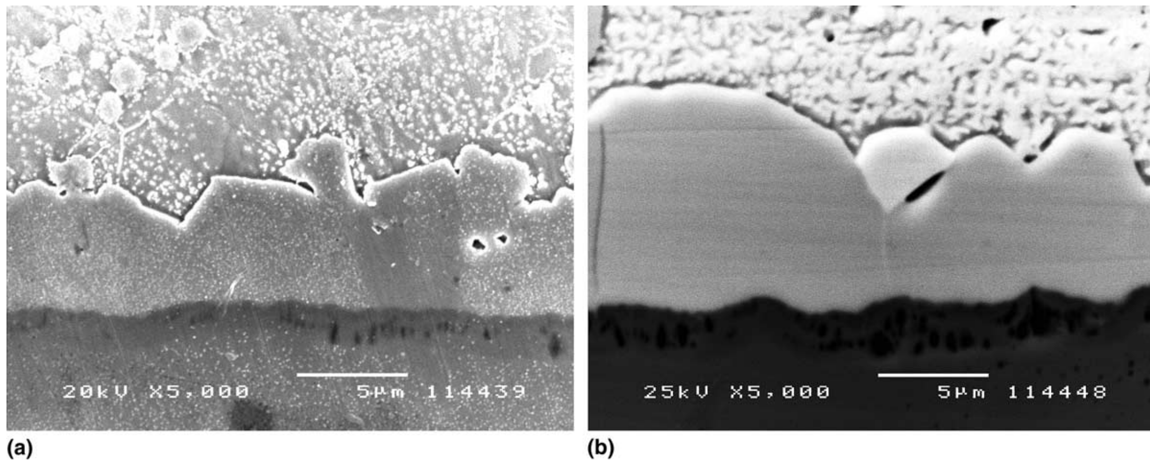

Fig. 7. Kirkendall voids formed in samples of Sn–3.5Ag solder with Ni–P UBM aged at 216 °C. (a) 16 h. (b) 225 h.

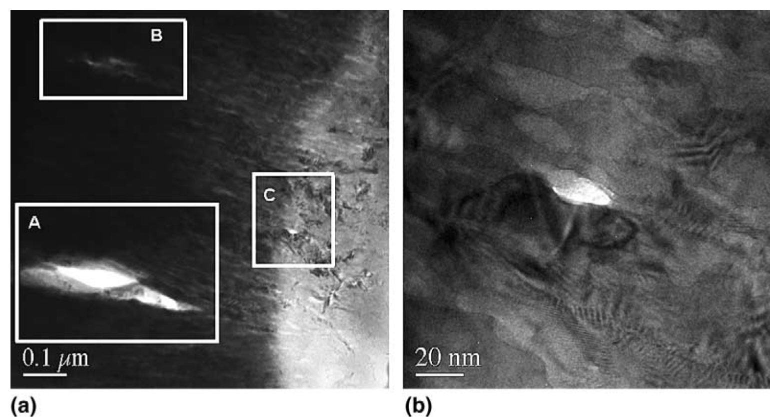

Fig. 8. Kirkendall voids inside Ni_3P layer in Sn–3.5Ag with Ni–P UBM sample aged at 150 °C for 100 h. (a) Kirkendall voids at locations A, B and C. (b) High magnification view of location C.

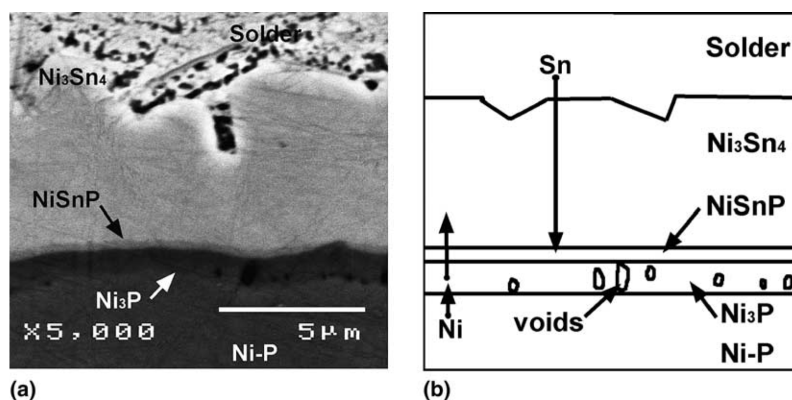

Fig. 9. NiSnP layer between Ni_3Sn_4 and Ni_3P layers in Sn–3.5Ag sample aged at 190 °C for 400 h. (a) SEM micrograph. (b) Schematic diagram.

Ni_3Sn_4 layer. TEM picture (Fig. 10(a)) revealed a clear transition from the laminar Ni_3P morphology to an equiaxial nano-crystalline NiSnP region. A composition profile using EDX analysis (with a beam size of 10 nm) was performed with the TEM facility. The analysis was carried out from point A to B, as labeled in Fig. 10(a), crossing both NiSnP and Ni_3P layers with a step size between 30 to 50 nm. It is interesting to note from the results, as shown in Fig. 10(b), that the Sn concentration varies inside the NiSnP layer with locations close to Ni_3Sn_4 side containing larger amount of Sn. There is sudden termination of Sn at the NiSnP/Ni_3P interface.

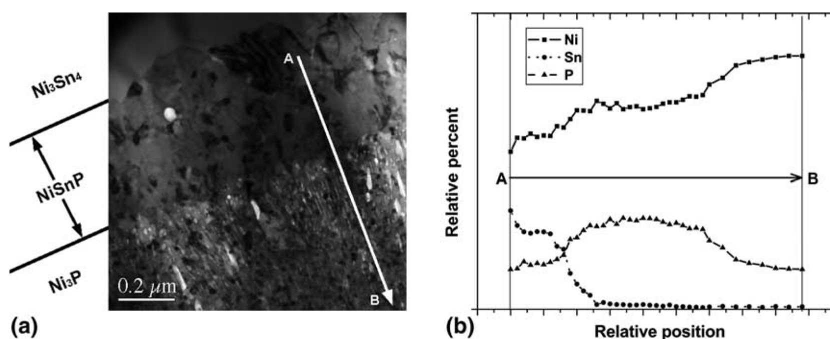

Fig. 10. (a) TEM picture showing the micro-structural difference between the Ni_3P layer and the NiSnP layer. (b) Ni, Sn and P composition profiles using EDX analysis from point A in the direction of arrow in (a).

4. Discussion

4.1. IMC growth kinetics in solid-state reaction

The linear relationship between the IMC thickness and $(\text{time})^{1/2}$ suggests that the IMC growth is a diffusion controlled process. The relationship can be represented by

$$\delta = \delta_0 + k\sqrt{t}, \quad (1)$$

where δ and δ_0 are the thickness of the IMC at time t and zero, respectively, and k is the growth rate constant. According to the classical kinetics theory, the variation of k with temperature can be represented by the Arrhenius equation

$$k = A\exp(-Q/RT), \quad (2)$$

where A is a prefactor, T is the absolute temperature, R is the gas constant and Q is the activation energy of the reaction.

An Arrhenius plot, as shown in Fig. 11, is obtained for the two solder/UBM systems from the data in Table 1. The activation energy for the Ni_3Sn_4 growth in solid-state reaction for Sn–3.5Ag solder is estimated to be 110 kJ/mol, and the one for Sn–37Pb solder is 141 kJ/mol. The pre-exponential coefficients are 0.218 and 676 cm^2/s for Sn–3.5Ag and Sn–37Pb solders, respectively. Predicted by Fig. 11, the growth rate for Sn–37Pb with Ni–P UBM will overtake the one for Sn–3.5Ag for temperatures higher than 190 °C, but this temperature is beyond the melting temperature for the eutectic SnPb solder. Therefore the IMC growth rate is higher with Sn–3.5Ag/Ni–P system than Sn–37Pb/Ni–P system for practically the whole comparable range of solid state Ni–Sn reactions, and the lower the thermal aging temperature, the larger the difference in their growth rates.

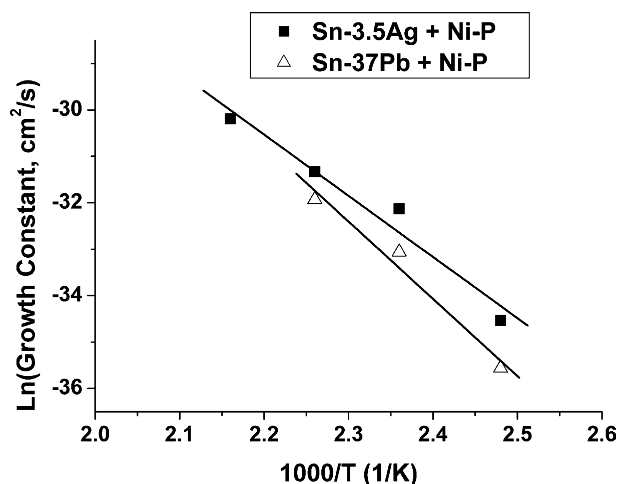

Fig. 11. Arrhenius plot for the formation of Ni_3Sn_4 between Sn-rich solders and Ni–P UBM.

4.2. Effect of solder composition on IMC growth

Lead in the eutectic Sn–Pb solder is not present in the intermetallics although it is an indispensable ingredient in the solder systems. The addition of 37 wt% Pb decreases the activity of Sn and affects the Sn/UBM reaction [19]. With extended aging, more and more Pb accumulates at the interface, forming a layer consisting of the so-called Pb-rich phase [20–22]. Further diffusion of Sn to the interface has to go through this layer, leading to further reduction in Sn activity at the solder/UBM interface. Therefore it is not surprising for engineers and researchers to come to realize that all the lead-free solders containing more than 90 wt% Sn poses higher risk of IMC over-growth. In fact one of the reliability concerns for the application of lead-free solders is how to slow down its IMC growth by designing suitable solder/UBM alloy systems. Our current work verifies that the IMC growth is much faster with Sn–3.5Ag than Sn–37Pb. The accumulation of Pb-rich phase at the solder/Ni_3Sn_4 interface may be responsible for the difference in Ni_3Sn_4 activation energy for the two solders.

Silver in Sn–3.5Ag solder forms Ag_3Sn IMC particles randomly distributed inside solder matrix upon cooling, as seen in Fig. 1(a). Under extreme condition of long time reflow followed by fast cooling, tiny Ag_3Sn particles may also nucleate heterogeneously on the surface of

Ni_3Sn_4 IMC. The formation of Ag_3Sn IMC will not be discussed in detail in this work since it is largely formed in the solder matrix rather than at the interface. As the amount of Ag is small, it is not likely to have a major effect on Sn–Ni interfacial reaction.

4.3. Kirkendall voids in Ni–P UBM system during solid state reaction

The formation of Kirkendall voids inside the Ni_3P layer can be observed at both Sn–3.5Ag and Sn–37Pb solder/Ni–P UBM interfaces. No such voids were found at the interfaces of the sputtered pure nickel UBM systems [18]. Therefore the P in electroless Ni–P UBM, or to be more specific, the presence of Ni_3P layer between intermetallics and UBM is solely responsible for the voids formation.

A deliberation on the formation mechanism is given below. At the very beginning of solder reaction the formation of Ni_3Sn_4 causes depletion of Ni from the surface of the electroless Ni–P UBM. This would result in the formation of crystalline phase of Ni_3P [10]. Further supply of nickel for the Ni_3Sn_4 to grow may come from two sources, decomposition of Ni_3P at the reaction front or the diffusion of nickel from the unreacted Ni–P through the Ni_3P layer. If Ni_3P decomposes and the decomposed Ni diffuses through Ni_3Sn_4 to react with Sn, there would be three possible destinations for the decomposed P in this reaction: it may either diffuse through Ni_3Sn_4 to reach solder matrix, or stay at the front of Ni_3P layer to form a much high P concentration layer, or to diffuse through Ni_3P layer back to Ni–P UBM. In our research, no P has been detected inside the solder. Neither has a high P content layer between Ni_3Sn_4 and Ni_3P been found. Therefore the first two options are not possible. For the third option to occur, i.e., P diffuses back to the interface between Ni_3P and electroless Ni–P, no voids would be formed. This option was depicted by Jang et al. [10] as they did not observe any voids at the interface. Upon re-examining their work, we believe that the short reaction time used in their study is probably the reason that they were unable to observe any voids. Negating the possibility of decomposition of Ni_3P, the void formation can only be explained by the net nickel diffusion out through Ni_3P layer while there is not enough compensation from other elements to fill the vacant sites left by nickel.

The well-developed fine columnar structure in the Ni_3P layer was also observed by other researchers on similar solder/UBM systems [5,10,23]. This layer plays an important role in element diffusion and voids formation. Diffusion along the columnar grain boundaries is relatively easy. On the other hand, it is interesting to observe that Sn element stops at the interface between the NiSnP layer and the Ni_3P layer (Fig. 10(b)). The existence of this thin, yet morphologically and compositionally distinctive layer indicates that Sn can diffuse through Ni_3Sn_4. It is probably due to higher diffusion rate of Ni towards the solder, as well as the formation the ternary NiSnP layer, that prevents Sn from reaching the Ni–P UBM. In other words, there is a net out-flux of Ni both from Ni–P UBM to Ni_3P layer and from Ni_3P layer to Ni_3Sn_4 IMC. This has resulted in the formation of voids inside Ni_3P layer at both locations close to NiSnP layer and Ni–P UBM. Driving force for the Ni flux is the concentration difference between the neighboring layers, which is clearly shown in Fig. 10(b). Concentration of Ni is higher in Ni–P UBM than in Ni_3P layer. When Ni diffuses from Ni–P to Ni_3P layer, vacancies diffuse from Ni_3P layer to Ni–P simultaneously. Because the Ni–P has an amorphous microstructure, it is very difficult for vacancies to diffuse into Ni–P layer before it crystallizes to Ni_3P. As a result, vacancies accumulate at the interface of Ni_3P/Ni–P and grow to voids. Volume of these voids increase with the crystallization process of Ni–P in the solid state reaction between Ni–P and solder. With the presence of Kirkendall voids inside the Ni_3P layer, the element diffusion becomes easier through the free surface of the voids as well as through the grain boundaries. With extended aging time, the nucleated voids grow to a larger size and become observable under SEM or even optical microscope.

Our understanding for the interfacial reactions between Sn-containing solders and electroless Ni–P metallization during thermal aging is summarized in the schematic drawing shown in Fig. 9(b). Sn diffuses through Ni_3Sn_4 to reach the interface with Ni_3P and form a NiSnP layer. Ni diffuses out from Ni–P to react with Sn. Thickness of Ni_3Sn_4 layer increases because of Ni and Sn diffusion during thermal aging. Ni out-diffusion results in enrichment of P, triggering the formation of a layer consisting of nanocrystalline Ni_3P layer. Voids nucleate at the initial stage of solder reaction and keep on growing in solid state reaction between solders and Ni–P UBM.

Formation of Kirkendall voids has also been observed by other researchers with different process parameters or materials. Hung et al. [11] reported the voids in Sn–Pb solder/Ni–P sample reflowed at 220 °C for 90 min. The amount of the voids was found to have increased with reflow time. In a study on the interaction of Sn–Ag solder with Ni–P UBM during reflow, Jeon et al. [17,24] found Kirkendall voids present inside the Ni_3Sn_4 phase close to the P-rich layer. They attributed the void formation to the fast diffusion of Sn from the IMC towards the Ni–P UBM. In the SnAgCu/Ni–P system reflowed for five times, Zeng et al. [1] observed voids in the NiSnP layer. Their explanation to void formation is that in-flux of Sn is much smaller than the out-flux at $(Cu, Ni)_6Sn_5/Ni_3P$ interface. In

spite of these discrepancies, it seems reasonable to conclude that the presence and locations of the Kirkendall voids depend on a few factors or a combination of them: Ni–P UBM with Sn containing solder, prolonged reflow or multi-time reflow and/or long time aging at relatively high temperatures.

Kirkendall voids used to be a serious reliability concern in the wire bonding technology. The unbalanced diffusion fluxes of aluminium and gold through the intermetallic compound phases results in the materials depletion in certain areas which affects the mechanical integrity of the wire bond joints. Voids in the Ni_3Sn_4 layer of SnPb solder joints were reported by Jeon et al. [17,24] to have a detrimental effect on joint reliability. With increasing reflow time, the cracks propagated into Ni_3Sn_4 layer and voids were found on the fracture surface. This indicates that the IMC layer with Kirkendall voids inside is an easy path for crack propagation, resulting in brittle fracture. To what extent the Kirkendall voids in the Sn–3.5Ag solder with Ni–P UBM will affect the performance and reliability of flip chip packages is not clear yet. Investigation is on going in the authors' labs to clarify their influence to the mechanical and electrical properties of solder joints.

5. Conclusions

In this study, we compared the morphology of the intermetallic compounds formed between Sn-containing solders (Sn–3.5Ag and eutectic Sn–Pb) and electroless Ni–P UBM. The IMCs formed by the Sn–3.5Ag solder exist in chunky crystal blocks and small crystal agglomerates, while that by the SnPb solder exhibits similar shapes but in smaller sizes. Three distinctive layers, Ni_3Sn_4, NiSnP and Ni_3P, exist between Sn-containing solders and Ni–P UBM as a result of Sn/Ni–P reaction. All three layers are dominated by crystalline phases. The exact crystal structure of the ternary NiSnP is yet to be identified. Thermal aging resulted in growth of the intermetallics both in terms of overall thickness and crystal grain sizes. The thickness of the Ni_3Sn_4 layer was found to increase linearly with the square root of thermal aging time, indicating that the formation reaction of the IMCs is a diffusion controlled process. The activation energy for Ni_3Sn_4 growth in solid state reaction is found to be 110 and 141 kJ/mol for Sn–3.5Ag and Sn–37Pb solder, respectively. The IMC grows faster with Sn–3.5Ag solder than with eutectic SnPb solder. Kirkendall voids were found inside Ni_3P layer in both solder systems. These voids are the results of net out-flux nickel diffusion and will affect the reliability of the solder joints. The kinetics of Kirkendall voids formation and its implication to the mechanical integrity of the solder joint need to be studied in the future.

Acknowledgements

This work was supported by an Academic Research Fund from Nanyang Technological University. Helpful discussion with Dr. Andriy Gusak and Dr. D.L. Butler is gratefully acknowledged.

References

[1] Zeng K, Tu KN. Six cases of reliability study of Pb-free solder joints in electronic packaging technology. Mater Sci Eng 2002;R38:55.
[2] Tu KN, Zeng K. Tin–lead (Sn–37Pb) solder reaction in flip chip technology. Mater Sci Eng 2001;R34(1):1.
[3] Liu AA, Kim HK, Tu KN. Spalling of Cu_6Sn_5 spheroids in the soldering reaction of eutectic SnPb on Cr/Cu/Au thin films. J Appl Phys 1996;80(5):2774.
[4] Kim HK, Tu KN, Totta PA. Ripening-assisted asymmetric spalling of Cu–Sn compound spheroids in solder joints on Si wafers. Appl Phys Lett 1996;68(16):2204.
[5] Liu PL, Shang JK. Thermal stability of electroless-nickel/solder interface: part A. Interfacial chemistry and microstructure. Metall Mater Trans A 2000;31A(Nov):2867.
[6] Chan YC, Tu PL, Tang CW, Hung KC, Lai KL. Reliability studies of μBGA solder joints – effect of Ni–Sn intermetallic compound. IEEE Trans Adv Pack 2001;24(1):25.
[7] Lin KL, Liu YC. Reflow and property of Al/Cu/electroless nickel/Sn–Pb solder bumps. IEEE Trans Adv Pack 1999;22(4):568.
[8] Mei Z, Dauskardt RH. Reliability of electroless processed thin layered solder joints. In: MRS Spring Meeting Symposium M; Materials Reliability in Microelectronics IX; 1999. p. 1.
[9] Lee CY, Lin KL. The interaction kinetics and compound formation between electroless Ni–P and solder. Thin Solid Films 1994;249(2):201.
[10] Jang JW, Kim PG, Tu KN. Solder reaction-assisted crystallization of electroless Ni–P under bump metallization in low cost flip chip technology. J Appl Phys 1999;85(12):8456.
[11] Hung KC, Chan YC, Tang CW, Ong HC. Correlation between Ni_3Sn_4 intermetallics and Ni_3P due to solder reaction-assisted crystallization of electroless Ni–P metallization in advanced packages. J Mater Res 2000;15(11):2534.
[12] Hung KC, Chan YC. Study of Ni_3P growth due to solder reaction-assisted crystallization of electroless Ni–P metallization. J Mater Sci Lett 2000;19:1755.
[13] Liu PL, Shang JK. A comparative fatigue study of solder/electroless-nickel and solder/copper interfaces. J Mater Res 2000;15(11):2347.
[14] Lee CY, Lin KL. Bonding fracture mechanism between Sn–37Pb solder and electroless nickel alloy deposits. INTERpack 95 1995;2(March):26.
[15] Kulojarvi K, Vuorinen V, Kivilahti J. Effect of dissolution and intermetallic formation on the reliability of FC joints. Microelectron Int 1998;15(2):20.
[16] Jang JW, Peter DR, Lee TY, Tu KN. Morphology of interfacial reaction between lead-free solders and electroless Ni–P under bump metallization. J Appl Phys 2000;88:6359.
[17] Jeon YD, Paik KW, Bok KS, Choi WS, Cho CL. Studies on Ni–Sn intermetallic compound and P-rich Ni layer at the electroless nickel UBM-solder interface and their effects on flip chip solder joint reliability. In: Electronic Components and Technology Conference, IEEE; 2001.
[18] Qi GJ, He M, Chen Z. Reaction of Sn-bearing solders with nickel based under bump metallizations. In: Proceedings of the Yazawa International Symposium, in Conjunction with the 132nd TMS

Annual Meeting and Exhibition, 2–6 March 2003, San Diego, vol. 1. p. 1173.
[19] Trumble B. Lead-free electronics come of age. IEEE Spectrum 1998:55.
[20] Lee KY, Li M, Olsen DR, Chen WT. Microstructure, joint strength and failure mechanism of Sn–Ag, Sn–Ag–Cu versus Sn–Pb–Ag solders in BGA packages. In: Electronic Components and Technology Conference; 2001.
[21] Ho CE, Chen WT, Kao CR. Interactions between solder and metallization during long-term aging of advanced microelectronic packages. J Electron Mater 2001;30(4):379.
[22] Lee KY, Li M. Formation of intermetallic compounds in SnPbAg, SnAg, and SnAgCu solders on Ni/Au metallization. Metall Mater Trans A 2001;32A:2666.
[23] Zeng KJ, Vuorinen V, Kivilahti JK. Interfacial reactions between lead-free SnAgCu solder and Ni(P) surface finish on printed circuit boards. IEEE Trans Electron Pack Manufac 2002;25:162.
[24] Jeon YD, Paik KW, Bok KS, Choi WS, Cho CL. Studies of electroless nickel under bump metallurgy – solder interfacial reactions and their effects on flip chip solder joint reliability. J Electron Mater 2002;31:520.